Materials Horizons

ROYAL SOCIETY OF CHEMISTRY

COMMUNICATION

View Article Online
View Journal

Cite this: DOI: 10.1039/d5mh01507c

Materials derived from a sulfur vulcanization of biochar

Chaza Al Akoumy,[a] Mohamed Amine Mezour[b] and Richard Martel *[a]

Received 7th August 2025,
Accepted 10th November 2025

DOI: 10.1039/d5mh01507c

rsc.li/materials-horizons

The pyrolysis of lignocellulosic biomass yields biochar consisting of high-carbon scaffolds bearing a variety of functional groups. As produced, the biochar is mechanically fragile and lacks the structural cohesion needed for making structural materials. To enhance both its chemical stability and mechanical strength, elemental sulfur is here introduced to induce a vulcanization reaction with biochar. Heating a biochar–sulfur (BS) mixture up to 185 °C under pressure induces effective crosslinking within the carbon network of biochar, a reaction attributed to free-radical sulfur polymerization and addition to functional groups attached to the carbon network of biochar. The synthesis method yields a crosslinked biochar with markedly enhanced mechanical strength. Depending on the synthesis conditions, the compressive strength and Young's modulus can reach values between 22–382.5 MPa and 6–165 GPa, respectively. With the density of only 1.4 g cm^{-3}, the mechanical properties of the best synthesized materials closely match that of structural steel. The BS materials can potentially be used as sustainable materials in parts and products for human infrastructure and transport. Alternatively, this method may also provide an alternative pathway for biomass-derived carbon storage contributing to climate change mitigation.

New concepts

This work introduces the concept of a sulfur-volcanized biochar (BS materials) and presents a cheap and simple method of synthesis in batches on a few grams scale. The mechanical properties of synthesized BS materials surpass that of other biomass-derived materials. Depending on the starting composition, the results show mechanical strength values reaching that of hard plastic and even structural steel. The properties measured so far suggest that the BS material is of potential interest to make parts across various industries for use in infrastructure and transportation. More importantly, this work presents a low-cost and sustainable method to prepare hard and stable materials using only sulfur and biochar without solvent or additives.

1. Introduction

Reducing atmospheric CO_2 will require innovative approaches in various fields of science to address key milestones for future human development, such as favoring sustainable materials, reducing energy consumption, switching to lower-carbon fuels, increasing renewable energy sources and agro-sequestration of crops, to name just a few.[1–4] The biochar is a biomass-derived material produced from the oxygen-free thermal combustion of organic raw and residual materials, such as wood, shrimp shells, algae, *etc.* Due to its high carbon content and low oxygen (≈5%) or nitrogen (≈0.1%) levels, biochar has been considered as one of the most abundant carbon feedstocks for material synthesis, ensuring both sustainability and CO_2 removal.[5] Although promising, a direct use of biochar in the formulation of next generation materials has been limited so far by both chemical and technical issues, including a poorly defined reactivity and a large variability of morphology and composition depending on the synthesis conditions and biosources. Tailoring the surface functionalities of biochar is therefore a key ingredient in deriving functional materials from biochar.[6] For example, the biochar has been modified to prepare cheap media for the adsorption of heavy metals and pollutants, and to serve as solid support and catalyst centers in heterogeneous catalysis.[7] The biochar has also been functionalized for use in electrochemical applications, thanks to its enhanced electrical conductivity in higher pyrolysis conditions and fairly good cationic exchange capacity.[7] A recent demonstration has shown, for instance, that a biochar derived from lignin can constitute a viable replacement for carbon black in the anode formulation of a lithium-ion battery.[8]

The potential use of biochar in structural materials can open a wider range of applications, but this development has been mitigated by important limitations, giving few examples of use as a filler and only rare cases as a binder. The biochar is highly porous and brittle, which mostly explains the poor mechanical

[a] Department of Chemistry and Institut Courtois, University of Montreal, Montreal, Quebec H3C 3J7, Canada. E-mail: r.martel@umontreal.ca
[b] Elkem Biocarbon, Chicoutimi, Canada

performance[9] of the as-produced biochar. It has shown limited benefits as a filler in plastic and concrete-based composites, which are considered as marginal below 3–10 wt% and detrimental above that threshold.[10–12] These limitations have been ascribed to the poor adhesion properties of biochar and a generally poor control over its surface chemistry. To improve mechanical strength and make biochar-derived materials more robust structurally, one needs to achieve both a good filling of the pores and a crosslinking of the carbon backbone across the matrix. For this purpose, we have selected elemental sulfur (S_8), which is abundant, cheap and widely available as a residue of the petroleum refining processes.[13] In mild conditions, sulfur generates species that can react with a wide range of organic moieties, thanks to the dynamic nature of S–S bonds and a two-electron chemistry, in which sulfur can participate as both electrophile or nucleophile.[14] Elemental sulfur forms a yellow liquid at around 140 °C and cleaves homolytically by simple heating to ~159 °C, giving a transition to darker red. The latter triggers an equilibrium ring-opening polymerization (ROP) that forms linear polymers through direct couplings between diradical chain ends (Fig. 1(A)).[15] The ability to become liquid and form ROP and S–C bonds on various chemical functions upon heating, with that of being cheap and abundant, makes sulfur an excellent candidate for inducing reticulation in biochar. The C–S and S–S bonds considered here are strong covalent bonds with bond breaking energy of 272 kJ mol^{-1} and 226 kJ mol^{-1}, respectively.[16]

Here, we present a synthesis route of biochar–sulfur (BS) materials, which can also be defined as a sulfur–vulcanized biochar. Prepared in the shape of a pellet, the BS material is produced by heating in two steps inside a pressure mold under a controlled atmosphere. We report that liquid sulfur readily fills the pores of the biochar and induces a crosslinking reaction under pressure, which in turn collapse the matrix and transforms synergistically biochar into a hard and solid material. The experiments with BS pellets demonstrate that the reaction creates a reticulated network of S–S and C–S interatomic bonds that enhance the mechanical properties of biochar (Fig. 1). The biomass source of biochar used here is pine wood residue from the manufactures of furniture, but the method is likely transferable to many other types of biochar.

2. Results

We developed a proof of concept of BS materials using different mixtures of biochar and sulfur prepared using the simplest and cheapest approach possible. Biochar is carbon-rich and porous, and disposes of a rather limited oxygen content (~20%, see Table S1). Its complex chemical structure carries functional groups and some aromaticity, which are accessible thanks to a high specific surface area and open porosity. The surfaces are mostly composed of oxygenated functional groups, which confer to the as-produce biochar a complex chemistry and a level of reactivity that can vary from one source to another.[7] The presence of abundant functional groups at the surface makes biochar's chemistry complex, but the reactivity can be further modified by physical (heat, oxidative gas adsorption, *etc.*) or chemical treatments (*e.g.* acid impregnation).[17] As illustrated in Fig. 1(A), the chemical reactivity can be modified by simple heating in a reactor up to 200 °C. Such heat treatment is known to lead to an overall decomposition of the organic phases, which increases carbon content and further develops a network of micropores distributed inside the biochar matrix.[18] In the presence of air, heat treatments also favor oxygen adsorption at

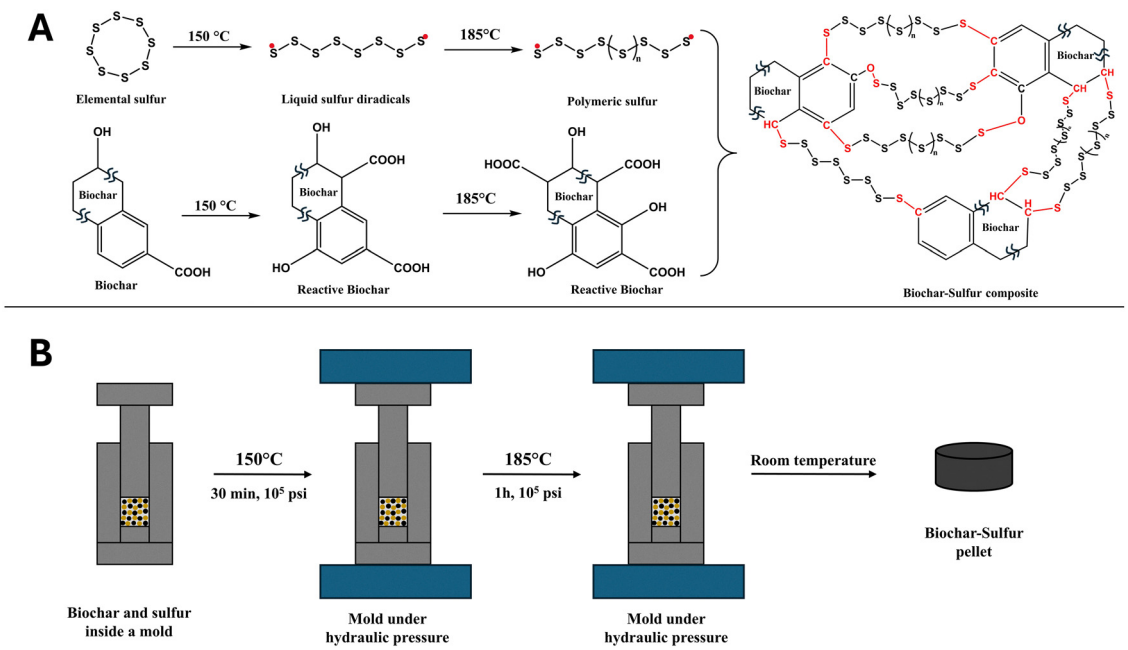

Fig. 1 Synthesis route of a biochar–sulfur pellet: (A) schemes of the chemical reaction of biochar and sulfur during the preparation, (B) experimental steps of preparing biochar–sulfur pellets.

the biochar surface, which further increases its reactivity.[19] Fig. S1A shows infrared absorption spectra (FTIR) of unmodified biochar after various thermal treatments. The initial material is rich in carbon and gradually acquires a higher content of oxygen-containing functional groups, as evidenced by an increase of vibrational peak intensity at 1031–1097 cm^{-1} (C–O–C), 1459 cm^{-1} (–COOH and –CHO), 1559 cm^{-1} (aromatic C–C), 1650–1659 cm^{-1} (C═O), 1718 cm^{-1} (C═O), and 3420–3447 cm^{-1} (–OH). This increased reactivity has also been checked by thermal gravimetric analysis (TGA) (Fig. S1B) and electron spin resonance (ESR, Fig. S14). In TGA, the mass increases from 200 °C to ~350 °C and degradation gets faster when a thermal treatment was applied, which indicates again higher reactivity. In ESR, this increased reactivity is evidenced by a significant rise of the spin density measured after annealing to 200 °C in air, which is ascribed to the formation of organic free radicals at the surface of biochar.

Heating the BS mixture should therefore activate the biochar reactivity and promote reaction with sulfur species with some of the biochar's functional groups. However, S_8 changes properties when heated: It is liquid above 120 °C and starts to polymerize[13] between 156 °C and 200 °C (see schemes in Fig. 1(A)). Because biochar is porous and mechanically fragile,[9] the phase change to liquid sulfur allows for easy diffusion of the reactants into the cavities and pores located deeper inside the biochar matrix. To accelerate sulfur diffusion and activate crosslinking, a synthesis method (Fig. 1(B)) was devised using a hydraulic press that can add pressure to the mold while heating the reactant mixture. The procedure is as follows: The mixture of biochar and elemental sulfur was placed in a 1-inch diameter cylindrical mold and then compressed with a hydraulic press placed in direct contact with two heating plates on each side of the mold. The mold temperature was closely monitored using a thermocouple inserted at the bottom of the mold. The hydraulic press was set to 10^5 psi while heating to 150 °C, which induces a melting of elemental sulfur. The pressure on the mold readily reduces itself during this first stage to less than 10^2 psi, which clearly indicates that liquid sulfur has melted and penetrated the pores and voids between biochar particles. After 30 minutes, the mold was pressurized again to return to the original pressure (10^5 psi) and the temperature was increased to 185 °C. This procedure compresses further the particles of biochar together, reduces the size of the pores, expels the excess of liquid sulfur, and activates, at the same time, sulfur ROP and crosslinking reactions.

To explore the parameters impacting the mechanical properties of the pellets obtained by this methodology, the sulfur content was varied from 20% to 80% in mass in the biochar–sulfur mixture for a constant total weight of 6 g per pellet. Tests with only biochar and sulfur (no mixture) were also performed but no solid pellet could be formed without a mixture of both together. For each composition, a total of 6 samples were prepared and tested for statistics and reproducibility. Hereafter, these samples are labeled using the initial mass composition. For example, the BS(20 : 80) indicates a biochar : sulfur pellet initially prepared using 20% mass of biochar and 80% mass of elemental sulfur. Table 1 presents the main results for BS(60 : 40) and BS(20 : 80) (see additional data in Tables S4 and S5). The experimental parameters include the normalized mass loss ($\Delta m/m$) before and after reaction, the pellet density after reaction and the elemental analysis in atomic% after reaction. The density of sulfur (2 g mL^{-1}) is higher than that of biochar, which has a volume density of 0.6 g mL^{-1} (Table S1). Without considering the pores, the biochar has a skeletal density of 1 g mL^{-1} (Table S2). Increasing the sulfur content should therefore increase the density of the pellets. As expected, the density reported in Fig. 2(B) (black curve) increases after reaction in air from 1 to 1.2 g mL^{-1} for BS(80 : 20) and BS(60 : 40), respectively. However, increasing further sulfur content unexpectedly decreases the pellet density. For example, the density of BS(20 : 80) pellets is 0.90 ± 0.02 g mL^{-1} after reaction, which is lower than that of the BS(60 : 40) (1.22 ± 0.05 g mL^{-1}). In addition, the density remains below that of the skeletal biochar, irrespective of the sulfur content. This is the first evidence that the pressed biochar still contains empty pores. As presented next, a higher density is only obtained when the reaction is performed under a nitrogen flow (red curve). These unexpected results indicate that the presence of air may be detrimental and should be avoided for high-density material synthesis. A clear sign of parasitic reactions is the appearance in air of a blue flame around the mold (Fig. S2B), which suggests a production of gaseous SO_2, which is strongly exothermic.

To prevent oxidation, the home-made setup was modified by adding an enclosure surrounding the mold. This was made with two stainless-steel cylinders assembled as a chamber around the mold (Fig. S2A). The cylinders can slide on each other to accommodate the movement of the press without leaking gas to the atmosphere. This chamber has two inlets for gas and a thermocouple entry, allowing for a control of the atmosphere around the mold while monitoring the temperature (see Methods). Surprisingly, the pellets still show a significant mass loss after reaction under a nitrogen flow (Table 1). For example, the $\Delta m/m$ of the BS (20 : 80) pellets after reaction under both nitrogen and air is 70–75%. Nevertheless,

Table 1 Mass loss, density and elemental analysis of biochar : sulfur pellets: BS(60 : 40) and BS(20 : 80) prepared in air and under nitrogen flow

Sample	$\Delta m/m^a$ (g) (%)	Density (g ml^{-1})	C at%	S at%	H at% ± 0.1	C/S ratio	C/H ratio
BS(60 : 40) in air	18	1.22 ± 0.05	59.9 ± 0.4	27.4 ± 0.6	2.5	2.2	28.6
BS(60 : 40) in nitrogen	18	1.19 ± 0.01	59.0 ± 1.4	25.4 ± 1.5	2.7	2.3	25.9
BS(20 : 80) in air	75	0.90 ± 0.02	50.3 ± 1.1	39.1 ± 1.5	2.1	1.3	24.0
BS(20 : 80) in nitrogen	71	1.37 ± 0.01	56.3 ± 0.7	29.0 ± 0.9	2.6	1.9	20.6

[a] $\Delta m/m$ = (mass before reaction − mass after reaction)/mass before reaction.

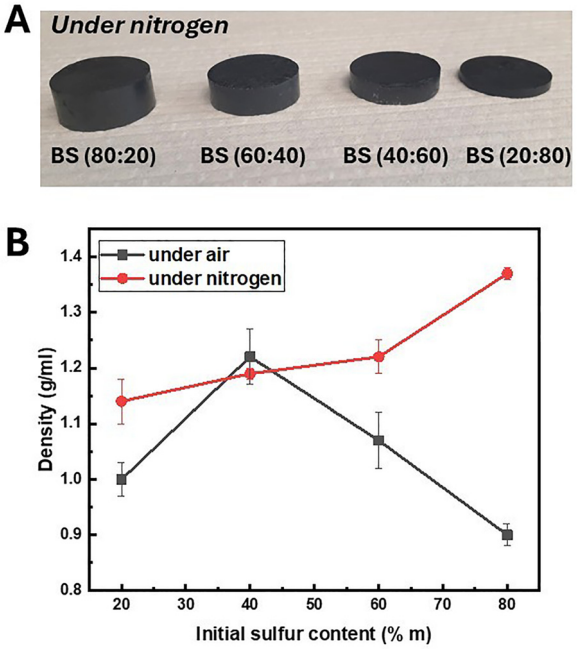

Fig. 2 (A) Photo of biochar–sulfur pellets prepared with different proportions of sulfur: 20%, 40%, 60% and 80% in mass, (B) variation in density as a function of sulfur content for pellets prepared under air (black) and under nitrogen (red).

the final density obtained with BS(20 : 80) under a nitrogen flow has increased to 1.4 g mL^{-1} (Fig. 2(B), red curve). The procedure under nitrogen gives smaller pellets after reaction (Fig. 2(A)) and thus provides higher density materials.

Further insight into the compositional changes is obtained using elemental analysis of the pellets produced in both conditions. The C and S contents (in atomic%) for the BS(60 : 40) and BS(20 : 80) pellets (Table 1) gives C/S ratios in the 1.3–2.3 range. As-received biochar shows a composition of 76.5 atomic% of carbon and 3.5 atomic% hydrogen (Table S1). The analysis therefore confirms that the significant mass loss is due to excess sulfur expelled from the mixture during reaction. This is true for all samples prepared in air and nitrogen, albeit the mass loss is particularly significant with the BS(20 : 80) pellets, for which most of the added sulfur has been removed from the pellet by the applied pressure. The reacted pellets are therefore composed of roughly 75–60 atomic% of biochar and 25–40 atomic% of sulfur, which exact values depend on the starting quantities and reaction conditions. These results also show that less than 30 atomic% of sulfur in the initial mixture may not provide enough sulfur to completely fill the pores and voids of the biochar used here. It is however not clear from elemental analyses alone if the sulfur has been protected from oxidation by the nitrogen flow. We noted for instance that some residual sulfur is left at the bottom of the mold after reaction, indicating that most sulfur that has leaked out of the mold gets oxidized outside the mold, probably into gaseous SO_2.

Visually, the BS(80 : 20) pellets prepared in air are brittle and show poor cohesion between particles. In contrast, the same composition prepared under a nitrogen flow gives a structurally

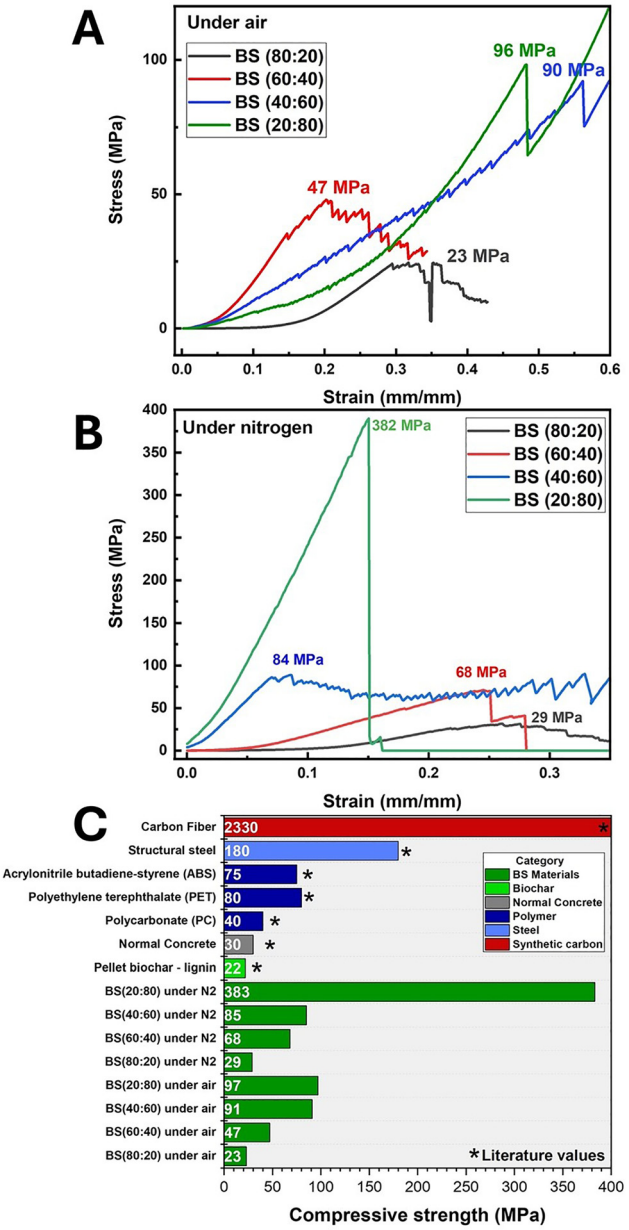

Fig. 3 Stress–strain curves using axial compression for biochar–sulfur pellets prepared with different amounts of sulfur following annealing (A) in air and (B) in a nitrogen flow. Compressive strength of the BS materials prepared in different conditions compared to that of other structural materials obtained from the literature and listed in Table S8 (C).

sound and hard solid (Fig. S3). Therefore, the nitrogen atmosphere plays an important role in enhancing the structural properties of the pellet. We argue that parasitic oxidative reactions may interfere with sulfur–biochar crosslinking reactions, as discussed next, giving chemical bridges across the pellets. For a more quantitative analysis, uniaxial compression tests were used to determine the mechanical properties of each pellet prepared in air and nitrogen conditions. The measurement consists of placing the pellet between two flat plates and applying a compressive load. As shown in Fig. 3 the compressive load is increased until the pellet deforms and finally

ruptures. The compressive load and displacement are measured simultaneously during compression, which is used to calculate the stress/strain data according to the compression-force dataset.[20] The results at small displacements show that the pellets deform elastically, giving a sublinear upward slope. The slope in this section of the curve is related to the Young's modulus. In this regime, the material deforms elastically, a behavior described as elastoplastic. At this point, the material starts to deform and the slope of the curve decreases. The curve continues its progression until reaching the maximum point when the pellet breaks. This point defines the breaking force, which is seen in Fig. 3 by sudden sawtooth jumps in the measured force. This is the compressive strength, namely the maximum force that the pellet can withstand before breaking, and therefore it represents its hardness. In total, the Young's modulus and the breaking force are good measures of the mechanical performance of the pellets.[21] Surprisingly, the simple synthesis route described above produces, in the right conditions, pellets exhibiting exceptional mechanical strengths. The BS(20 : 80) pellets prepared under a nitrogen flow in Fig. 3(B) gave compressive stress reaching up to 382 MPa, which is an interesting value for structural materials.

Fig. 3 compares the axial compression tests of the different pellets. In the air, the BS(80 : 20) pellet shows a modest breaking force of 23 MPa and a Young's modulus of 6 GPa (Fig. 3(A)). Increasing the initial sulfur content in the pellets improves the breaking force to 47 MPa for BS(60 : 40) and 97 MPa for BS(20 : 80) and the Young's modulus to 8 GPa and 12 GPa, respectively (Table S8). It is noteworthy to mention that most pellets prepared in air present multiple (non-elastic, discontinuous) yield point events along the strain movement, which are visible along the upturn curves. This suggests a non-uniform stress distribution across the pellet. The results with the pellets prepared under nitrogen are significantly improved. The breaking events have mostly disappeared, and the maximal breaking force is much higher: 29 MPa for BS(80 : 20) to 382 MPa for BS(20 : 80). The Young modulus goes from 5 GPa for BS(80 : 20) to 165 GPa for BS(20 : 80) (Table S8). These results further confirm the importance of the synthesis conditions on the mechanical performance of the pellets. What is surprising is the high mechanical performance of the best samples. The BS(20 : 80) shows for instance a very high elasticity of 165 GPa, which continues as an upward slope without deformation until a sudden failure at a very high breaking force of 383 MPa. This high value is interesting, as it exceeds that of plastics and is comparable to that of structural steel (Fig. 3(C)).

The BS(60 : 40) and BS(20 : 80) pellets were further tested using axial compression to compare the properties when only one pressure step at 150 °C is applied under nitrogen. Fig. S8 show lower mechanical properties compared to two pressure steps. For BS(60 : 40), the breaking force is about 24.47 MPa after one pressure step, while it increases to 68.05 MPa after the second step at 185 °C. The BS(20 : 80) is even more evident. The breaking force was 53.69 MPa after the first step at 150 °C and reached 382.6 MPa after the second step at 185 °C.

The chemical reactions and phase changes induced by heating were further investigated using differential scanning calorimetry (DSC). Fig. 4 summarizes the DSC results with BS(60 : 40) and BS(20 : 80) pellets, which have the best mechanical properties. As references, DSC measurements have also been performed on biochar and elemental sulfur and on mechanically mixed, but unreacted, biochar and sulfur samples (see also Fig. S9 and S10). In the following, these samples are labeled with B + S to specify the use of unreacted mixtures of biochar and sulfur.

In Fig. 4(A) (black curve), the DSC of biochar (no sulfur) shows no distinct thermal transition. Only a broad and irreversible endothermic peak is seen at around 100 °C, which is ascribed to water desorption. These results are fully consistent with *in situ* XRD measurements in Fig. S11, which confirms the presence of an amorphous phase during heating up to 300 °C. The reference DSC of elemental sulfur (Fig. 4(A) and Fig. S9, red curve) shows clear first order transitions at around 104 °C and 120 °C, which are assigned to phase transitions of crystalline orthorhombic (S_α) to the monoclinic phase (S_β) and of a melting of the S_β phase, respectively.[22] The experimental heat capacity of sulfur is $C_p \sim 0.6$ J (g K)$^{-1}$, which is near the literature value of $\sim$0.7 J (g K)$^{-1}$.[23] More importantly, the sulfur undergoes a homolytic dissociation at around 170 °C (ΔH_r = +348 J mole^{-1}, endothermic), which forms radical intermediates that polymerize in liquid sulfur into polysulfur chains.[24,25] This transformation is clearly seen in DSC. The residual sulfur recrystallizes upon cooling at low temperature (20–50 °C) back to the stable S_α phase and evolves in the subsequent heating/cooling cycle with only one clear melting transition of the S_α phase at 105 °C; the S_β phase is likely quenched by the polymeric phase.

Fig. 4(A)–(C) provides a direct comparison between the above reference DSCs and the reacted and mixed (*i.e.* unreacted) biochar–sulfur. For all samples, the thermograms are qualitatively similar to that of the starting materials taken separately but added together, except that the first order transitions of sulfur in BS samples appear sharper and at a slightly higher temperature (120 °C *vs.* 118 °C). This behavior is indicative of a change in the S_8 crystal size distribution, probably due to confinement into the pores of the biochar.[26] However, the heat capacity and transition enthalpies of reacted BS materials are reduced by a factor $\sim$2. For instance, the heat capacity of the BS(60 : 40) pellets is $C_p \sim 0.2$ J (g K)$^{-1}$, which is lower than that of sulfur and biochar. The enthalpy (normalized by the S content) of the transition at 120 °C is also reduced by about half. Using the ratio between the enthalpies of fusion, ΔH_f, of crystalline sulfur near 120 °C in the BS samples relative to that of the reference sulfur and neglecting amorphous phase formation, we estimate the unreacted sulfur is between 45% and 50% of the total mass of sulfur (see Table S9).

Direct evidence of exothermic crosslinking reactions could only be captured in DSC using a modified method to include a 90-minute isotherm at 120 °C during the first scan, which better matches the synthesis conditions (30-minute isothermal anneal at 150 °C during the first pressure step, see Methods). As shown in Fig. 4(D) (see also Fig. S10), this modified DSC

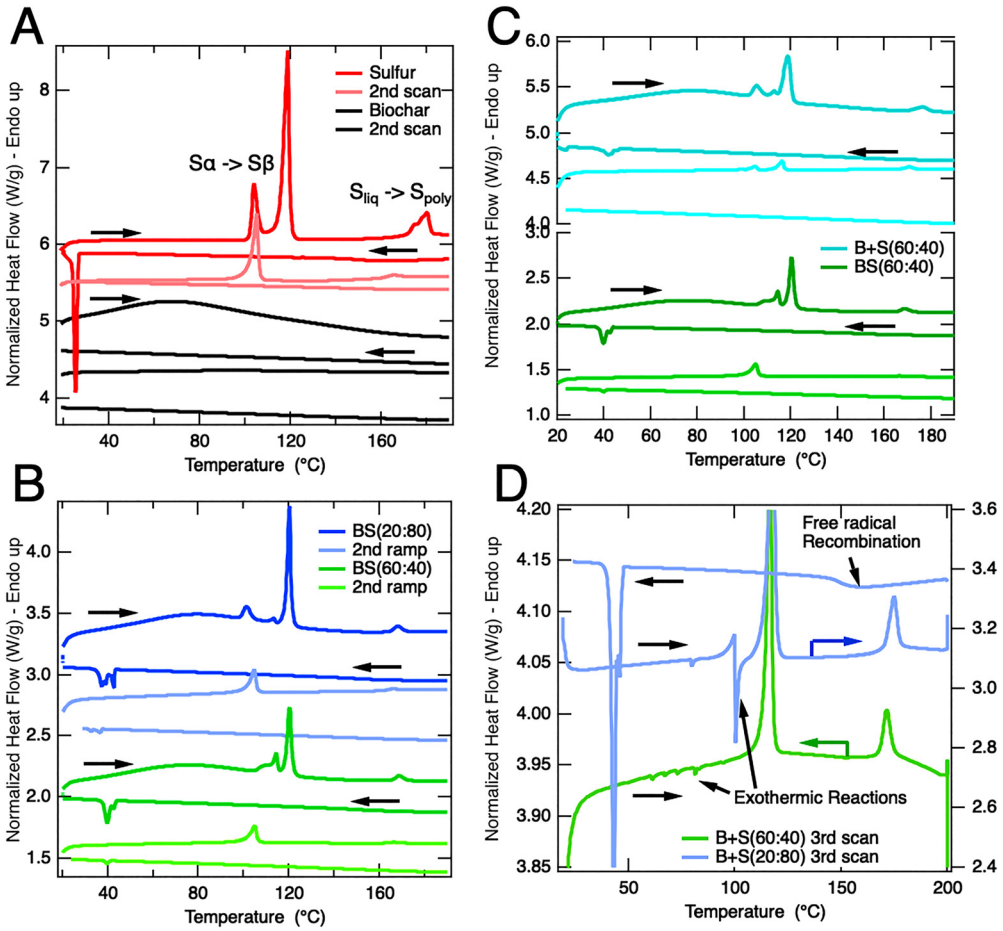

Fig. 4 DSC curves (10 °C min^{-1}) under a nitrogen flow of biochar (black curves) and elemental sulfur (red) compared to BS(60 : 40) (green), BS(20 : 80) (blue) and a mixture of biochar and elemental sulfur (B + S) before reaction. These DCS show thermal behavior during multiple (2 or 3) heating cycles as specified in the curves with each cycle offset below the first by steps of 0.5 W g^{-1}. (A) DSC scans of biochar compared to elemental sulfur. (B) DSC scans of sulfur compared to BS(20 : 80). (C) DSC scans in 20–200 °C range of sulfur compared to BS(60 : 40) and B + S(60 : 40). (D) DSC scans in 20–200 °C range of B + S(60 : 40) with the addition of a 120 °C isotherm for 90 min in the first cycle to highlight exothermic crosslinking events at low T.

protocol promoted clear exothermic events after the first heating scan up to 200 °C. Arrows in the figure highlight, for instance, exothermic events that occurred during the second scan of the B + S(60 : 40) sample between 35 °C and 110 °C. A more dramatic example of exothermic bursts occurred at 100 °C in the B + S(20 : 80) sample, which occurred near the fusion of the S_α phase. These delayed exothermic behaviors can be explained by diffusion-limited kinetics between unreacted poly-sulfur free radicals and various chemical groups at the surface of biochar. The first 120 °C isotherm promotes liquid sulfur diffusion towards the biochar surfaces before reaching the dissociation/polymerization reaction conditions at higher temperatures for the polymeric phase. Some of the free radicals that form at higher temperatures react with biochar, but the majority remains trapped in the matrix, requiring further diffusion by subsequent cooling–heating cycles. Fig. 4(D) shows, for instance, clear exothermic events near the phase transition (recrystallization/fusion) of the S_α phase, which appear to promote the diffusion of residual free radicals near biochar surfaces, giving delayed reaction. The exothermic signatures seen in mixed samples are absent in the reference samples. These exothermic events are only present when sulfur has been activated by temperature in contact with the biochar.

As an additional evidence of crosslinking, ESR measurements on BS(20 : 80) show a significant drop of the spin density after reaction (Fig. S14). That is, the ESR signal of biochar before reaction (g = 2.0037) dropped by a factor of 37 without shifting in position (g = 2.0028). The important change in intensity indicates a loss of most of the organic radicals (low spin–orbit coupling) in biochar, a reaction consistent with a sulfur bonding to the free radical species present at the surface of biochar. Additional ESR spectrum of BS(20 : 80) taken after 2 months show a slight decrease in signal, indicating a slow, yet ongoing, reaction process at room temperature within the pellets. This ESR response of sulfur reaction contrasts with that of a blank test with biochar only (no sulfur) heated to 200 °C, where a strong increase of ESR signal is observed at a shifted position (g = 1.9993), which implies a formation of different radical groups.

The thermal stability of the BS pellets was explored using TGA analysis (Fig. S13). Biochar (black curve) only starts to oxidize in the air at ~300 °C. A total loss of mass indicates the

complete oxidation of the carbon scaffold of biochar.[27] The presence of sulfur induces new thermal behaviours in the 100–125 °C, 160–200 °C and 250–300 °C ranges, which are near the crosslinking temperature. The oxidation of the sulfur is clearly seen in the TGA in the 200–250 °C region, where a mass loss of about 25% matches the sulfur content Table 1). The mass loss curves are also influenced by the quantity of added sulfur. The high temperature degradation in the TGA after 400 °C shifts from 461 °C for biochar only to 410–450 °C for biochar mixed with sulfur. This difference is explained by the different morphologies; the denser pellets are slightly more stable.

To better understand the role of the pressure steps on the morphology, SEM images of broken pellets were acquired after the first and second applied (10^5 psi) pressure steps at 150 °C and 185 °C, respectively (Fig. 5 and Fig. S5). These measures were completed with Mercury Intrusion Porosimeter (MIP) and X-ray tomography (Table S2 and Fig. S6). The biochar (no sulfur) in Fig. 5(A) and (B) maintains, after both steps, a dominant porous tubular structure that is typical of pyrolyzed pine wood.[28] The pure biochar pellets lack cohesion and remain powdery with MIP pore diameters between 0.6 μm and 32 μm. Comparing BS(60 : 40) and BS(20 : 80) samples after the first and second applied pressure steps at 10^5 psi reveals, however, different porosity and density values (Fig. S4). Macroscopically, the BS(60 : 40) and BS(20 : 80) samples after the first pressure step at 150 °C have thicknesses of 8.34 mm and 5.31 mm, respectively. After the second pressure step, they become 7.56 and 2.62 mm, respectively (Table S3). After the first pressure step at 150 °C, there are still some empty pores, which are seen by SEM in Fig. 5(C) and (E). More sulfur in the initial pellets gives a higher filling yield. MIP results (Table S2) confirm the SEM results: the porosity decreased from 66% to 12–18% after adding sulfur, confirming that the pores have been mostly filled by the liquid sulfur. In addition, the skeletal bulk density increased with the presence of sulfur from 0.97 to 1.28–1.35 g ml^{-1}, which is now explained by the inclusion of sulfur into the matrix. After the second pressure step, the porosity further decreased to 5.97% and the skeletal bulk density increased to 1.42 g mL^{-1} (Table S2). This is consistent with the SEM images showing the absence of pores (Fig. 5(D) and (F)). The surface of the pellets is visually smooth after the second step, and the pellets become very hard. X-Ray tomography images (Fig. S6) provide a three-dimensional view of the structure of the pore network across the entire pellet. It is clear that no pore is present throughout the pellets.[29] These results indicate that the first pressure step serves to diffuse the liquid sulfur into the pores, giving a reduced porosity down to 10%. The second pressure step at 185 °C compresses the pellets on itself, which collapses the pores and further reduces the porosity down to around 2–4% (Table S6). This step forces excess liquid sulfur to exit the pellet. Thanks to the ROP reaction of sulfur, the pellets can maintain their compact structure if enough sulfur is present, further indicating that a crosslinking process has been thorough throughout the pellet.

The presence of air alters the morphology and mechanical properties, and this can be further explored using X-ray tomography. Fig. S6 shows the presence of pores in all pellets prepared in the air, while no pore is observed under nitrogen. The higher the initial sulfur content, the higher the porosity of the samples prepared in the air (Table S6). The porosity in air is about 11%, which is higher than 2–3% under nitrogen. SEM images of some pellets prepared in the air (Fig. S5) confirm these observations. The question why the presence of air induces pores is not clear. We hypothesize that a full collapse of the pores cannot be maintained in the air due to lower crosslinking yields.

While infrared and Raman spectroscopy did not show clear signature of crosslinking (see details in Fig. S7), X-ray photoelectron spectroscopy (XPS) unambiguously showed formation of C–S bonding after reaction. The spectrum in Fig. 6(A) of as-produced biochar presents three features in the C1s region at 284.7 eV (C═C/C–C), 286 eV (C═O), and 288 eV (O═C–O). The reaction with sulfur only changes the intensities of the same peaks. The chemical transformation is however more visible in the S 2p region (Fig. 6(B)), which defines the environment of sulfur. That is, the S 2p region develops with new bands at 164 eV, 165 eV, 167.8 eV and 169.5 eV, corresponding to C–S, C═S, SO_3 and SO_4 respectively.[30] Importantly, the results show no S2p signal in as-received biochar and an increase of the C–S and C═S signals with the initial sulfur content from 40% to 80% in mass.

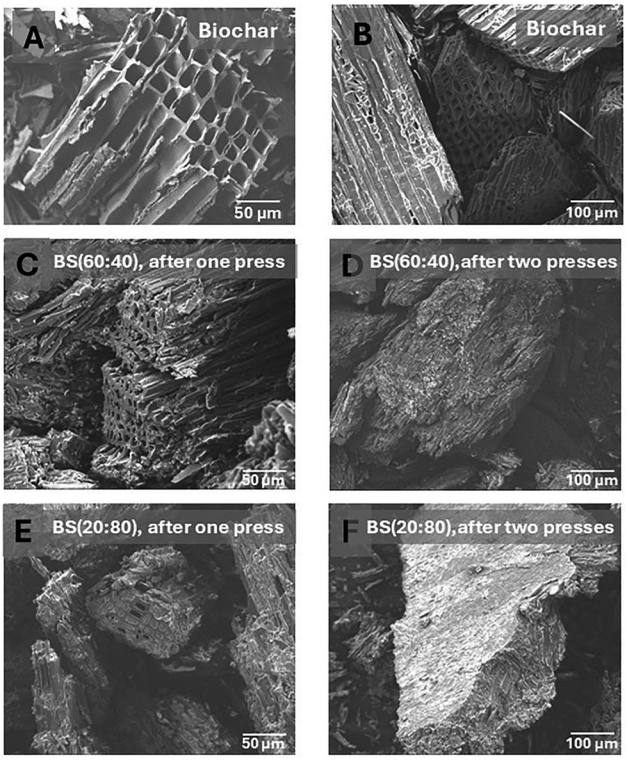

Fig. 5 SEM images of biochar (A), (B), biochar–sulfur pellets BS(60 : 40) (C), (D) and BS(20 : 80) (E) and (F) obtained under nitrogen. A, C and E were measured after the first pressure step at 10^5 psi and 150 °C. B, D and F were obtained after the second pressure step at 10^5 psi and 185 °C.

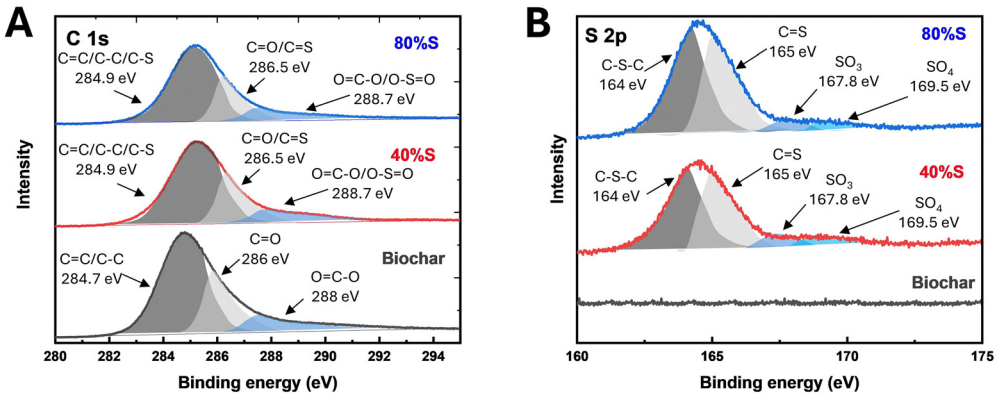

Fig. 6 XPS spectra of the C 1s (A) and S 2p (B) regions of biochar, BS(60 : 40) and BS(20 : 80).

3. Discussion

Together, these results provide information on the reaction pathways taking place during the two-pressure-step method described above. Increasing temperature in the first step to 150 °C induces a transition from the solid phase to the liquid phase of sulfur (Fig. 4(A)). The pressure is released during that step, probably because liquid sulfur flows into the pores or voids and diffuses freely at the biochar surfaces. This first step is above the fusion temperature of sulfur but below the homolytic fragmentation of sulfur, and no reaction is therefore expected during the first annealing step. Reestablishing pressure and increasing temperature in the second pressure step provide the conditions for crosslinking reactions. That is, cyclo-octasulfur (S_8) breaks down in the liquid phase into thiyl diradicals ($^{\bullet}S_8^{\bullet}$) at 159 °C and evolves with time to higher poly-sulfur diradicals.[31] Thiyl radicals is known to attack the poly-sulfur at this temperature chains and this reaction is fast compared to other reactions, such as S–C and S–O bond formations. This reaction is however complex and can also induce a depolymerization of poly-sulfur and other termination reactions that quench poly-sulfur chain propagation, a process often referred to as the backbiting mechanism.[32] However, the second pressure step collapses the pores of the biochar and forms a denser material while expelling any excess of liquid sulfur out of the pellet. This confinement of sulfur would significantly impede the backbiting mechanism in favor of other stable crosslinking processes at the surface of biochar. A higher temperature up to 185 °C further activates the homolytic fragmentation of the sulfur,[22] which may now occur deeper inside the biochar. Maintaining pressure is therefore an essential step to ensure biochar–sulfur interaction for the best cross-linking reaction between thiyl diradicals and biochar moieties, thus forming a plethora of S–S bridges terminated by S–O and S–C that covalently link the biochar backbone together across the entire BS matrix. Short and long polysulfide chains, which are now part of the matrix, are also stabilized against backbiting degradation by direct reaction with the biochar surface groups.

To explain the significant improvement in the mechanical properties of BS materials after cooling down, we speculate that the pressure confines sulfur and biochar together deep into the biochar matrix. The second pressure stage collapses the biochar onto itself, making upon heating thiyl radical attack more effective with the carbon backbone of the biochar. This provides higher cohesion between particles and better crosslinking yields after cooling down. The sulfur–biochar copolymerization discussed here is, therefore, a classical vulcanization of biochar. The reaction scheme also relates to the inverse vulcanization method introduced by Pyun and coworkers using vinylic monomers and other petroleum-based crosslinkers[33,34] and renewable monomers from biomass.[35] However, this biochar–sulfur chemistry is more complex in comparison and may also catalyses inverse vulcanization reactions, since biochar is known as a biogenic catalyst for sulfur polymerization.[36,37] Further investigations of the reaction parameters will allow gaining further insight into this vulcanisation chemistry and provide more quantitative values of the reticulation levels obtained with pressure, temperature and time. Here, the best mechanical properties are obtained for BS(20 : 80) samples, which have the highest sulfur initial content. This result highlights the need to carefully balance the quantity of sulfur for highest crosslinking yields.

Fig. 3(C) provides a visual comparison of the compressive properties measured with BS samples prepared with that in Table S7 of other commercial structural materials, such as structural steel, carbon fiber, concrete, and commercial plastics, *e.g.* polyethylene terephthalate (PET) and polycarbonate (PC). The BS(80 : 20) samples prepared in the air (compressive strength of 23.45 MPa) and under nitrogen (29.20 MPa) have already values close to that of a biochar pellet produced with lignin as a binder (22 MPa).[38] However, the compressive strengths of BS(60 : 40) and BS(40 : 60) prepared in air (47 MPa and 91 MPa) and under nitrogen (68 MPa and 85 MPa) are close to that of most commercial plastics (40–120 MPa).[39] Interestingly, the compressive strength of BS(20 : 80) significantly exceeds that of both commercial plastics and concrete (17–30 MPa).[40] The predominance of crosslinking with C–S bonds and S–S reticulation in this formulation is therefore clear. For example, the compressive strength of BS(20 : 80) pellets prepared in air (97 MPa) is slightly higher than those of commercial plastics, but the same composition prepared under nitrogen generates materials having an impressive compressive strength of 382.5 MPa. This value is higher than structural steel (*e.g.* AISI-SAE 1020) at ~180 MPa[41] and this important

result makes BS pellets interesting for eventual use in construction. The properties are still away from that of high performance commercial carbon fibers, which have compressive strengths of 2330 MPa,[42] but BS materials are likely to be much cheaper to produce on a large scale, given the current low prices of biochar and sulfur. Consistent with a good chemical stability, ESR results of a BS sample show that the spin density is low after reaction and remains mostly unchanged after 2 months (Fig. S14). In addition, our results show that the mechanical properties of the BS pellets did not change significantly after one year of aging. That is, the mechanical strength of BS(60 : 40) evaluated after few months to one year gives nearly the same properties: the compressive strength was 64 MPa after one year, compared to 68 MPa when freshly prepared. Comparing the Young's modulus of the BS pellets with that of commercial steel and concrete materials (Table S8), we found that BS(40 : 60) and BS(20 : 80) pellets prepared under nitrogen have Young's moduli from 5 GPa to 165 GPa, depending on the initial composition. The value of the best BS materials obtained is therefore much higher than that of concrete (28–41 GPa)[43] but slightly lower than commercial steel materials (190–210 GPa).[44] The only biochar–sulfur material published in the literature was made from straw biochar, lignin and sulfur as binders.[45] These materials showed, however, much lower compressive strength (1.5 MPa), which could be explained by the different chemistry used for fabrication.

Finally, the BS pellet synthesis is likely to release gaseous sulfur-containing compounds, such as liquid sulfur, H_2S and SO_2, which may be harmful to the environment. Analytical detection of SO_2 and H_2S was carried out during the preparation of BS(20 : 80). For SO_2 detection, the produced gas was bubbled through deionized water and analyzed using a pH meter (SO_2 can dissolve in water to form sulfurous or sulfuric acid). It was found that the pH slightly decreased from 6.7 to 6.27 during the BS(20 : 80) synthesis under nitrogen and further dropped to 6.07 in the air (Fig. S12A). A formation of SO_2 during synthesis is therefore observed, but we trust that this could be mitigated using a tighter control of the reactor designs to recover the excess of sulfur. For H_2S detection, the exit gas flow was bubbled through a 10 ppm methylene blue solution. H_2S forms soluble sulfide ions in the solution, which immediately reacts with methylene blue to form a complex that can be detected by UV-Vis spectra (redshifted peak). The experiment shows that H_2S is not detected during BS synthesis under either air or nitrogen atmospheres (Fig. S12B). Therefore, H_2S could be formed but only in very small quantities. This is consistent with the results in Table 1, in which there is no apparent drop of H content for both BS(60 : 40) and BS(20 : 80) pellets; *i.e.* a C/H ratio remains in a 20–28 range, which is similar to unreacted biochar.

4. Conclusion

Using this two-stage pressure method, biochar–sulfur materials were synthesized on a few grams scale at mild temperatures up to 185 °C. The reaction parameters were explored by changing the initial mass content of sulfur from 20% to 80% and controlling the atmosphere between air and pure nitrogen. The properties, morphology, structure, and mechanical properties of synthesized BS materials were all consistent with a crosslinking reaction between the sulfur and the carbon backbone of biochar. The preparation of BS pellets under air provided lower crosslinking yields and limited mechanical properties and some porosity (≈10%). Their compressive strength was between 23 and 96 MPa, which is like that of plastics and concrete. Under a nitrogen flow, the reticulation reaction is found to be more extensive, and the pellets present fewer pores (≈2%) and better mechanical properties. Up to 80% in mass, the more sulfur added, the higher is the mechanical properties. That is, the compressive strengths of BS(80 : 20), BS(60 : 40), and BS(40 : 60) pellets prepared under nitrogen were in the range of 29–84 MPa, which is similar to that of plastics (Fig. 3(C)). The BS(20 : 80) pellets showed a surprisingly high compressive strength of 382 MPa, which exceeds that of commercial structural steel at about 170 MPa. To our knowledge, the biochar–sulfur materials described here present among the highest mechanical performances obtained so far from bioresources, and there are no biocarbon-based materials discussed in the literature that rival these exceptional mechanical performances.

The BS materials are solely composed of biochar and sulfur, and it is fabricated using affordable conditions of pressure and temperature. The synthesis method is inexpensive, scalable and generates hard and lightweight materials that could be used in applications where mechanical performance, near that of metals or below, is required. The structural properties of the BS materials also suggest potential uses for construction and transport applications, or as fillers in reinforced composites, thanks to the presence of sulfur. One can also explore variant of the method in large batches using, for instance, compression molding that is often used in the industry. Because BS materials can be produced very cheaply, an interesting perspective is the storage of carbon and sulfur into structural materials, thus reducing both the anthropogenic carbon dioxide causing climate change and accumulated stocks of sulfur produced by petroleum refining processes. However, large-scale synthesis remains mostly unexplored and much other works will be needed to test more thoroughly other properties of BS materials, including aging, durability, wearing and fatigue during service, inflammability, toxicity, *etc.*

5. Materials and methods

The biochar, made from pyrolyzed pine wood saws, was provided by the Elkem Biocarbone. This biochar comes from a pilot plan located in Chicoutimi, Quebec, which uses moderate pyrolyse conditions for batch production, characterized by few second to minutes residence time in the pilot reactor at a temperature between 400 °C and 600 °C. Elemental sulfur was purchased from Fisher Scientific and used as received.

5.1 Preparation of biochar–sulfur pellets

Biochar and sulfur were mixed in different proportions from 20% to 80% for a total mass of 6 grams. The mixture was put into a cylindrical mold of 1 inch in diameter, and the mold was

pressed up to 10^5 psi and heated to 150 °C for 30 minutes under air. The mold was then pressed again at the same pressure and heated to 185 °C for one hour. After complete cooling, the pellet is removed from the mold. For the preparation under a nitrogen flow, the same procedure was followed in the same mold placed inside a stainless-steel cylinder, which forms an enclosure around the mold for atmosphere control under pressure. The cylinder has a gas tube inlet to ensure continuous flow of nitrogen around the mold and another inlet for thermocouples to monitor the temperature. The nitrogen flow is applied a few minutes before the procedure to clear residual air around the mold, and it is maintained during and after the reaction until the mold had completely cooled down. CAUTION: Heating elemental sulfur with other reactants can result in the formation of H_2S or other toxic gases. Temperature must be carefully controlled to prevent thermal spikes promoting uncontrolled reactions.

5.2 Material characterization

FTIR spectra were performed on a Bruker Vertex 80v Fourier transform spectrometer equipped with a KBr beam splitter and a deuterated alanine doped tri-glycine sulfate (DTGS) detector at a resolution of 4 cm^{-1}. Raman Renishaw Invia was equipped with a 514 nm laser and a 50× objective was used for the acquisition of Raman spectra and of optical images.

Thermal gravimetric analysis (TGA) was performed on a TGA 8000, PerkinElmer thermogravimetric analyzer under the air atmosphere, from 35 °C to 600 °C with a heating rate of 10 °C min^{-1} in air. Electron Spin Resonance (ESR) analyses were performed at room temperature using the X-band at 9.4 GHz on a Bruker Biospin Magnettech ESR 5000 instrument, with a 0.2 mT modulation amplitude at 100 kHz while scanning magnetic field in the range between 313–363 mT.

Elemental analysis of the carbon, hydrogen, nitrogen and sulfur contents in biochar–sulfur pellets was measured after reaction in triplicate using FlashSmart from Thermo Scientific analyzer. Briefly, 2 to 3 mg of each sample were combusted at 950 °C in the presence of oxygen. The gases formed (N_2, CO_2, H_2O, and SO_2) were separated by gas chromatography under helium and detected by an electrothermal detector. The instrument was calibrated with 2,5-bis(5-*tert*-butyl-benzoxazol-2-yl)thiophene (BBOT) and sulfanilamide was used as quality control.

Differential scanning clorimetry (DSC) was performed using a DSC6000 PerkinElmer instrument and Al_2O_3 crucibles for obtaining both heat capacities and phase transitions upon heating of various samples. The instrument was operated with sample weights of around 6 mg (in powder form). Two experimental methods were developed to study the thermal properties of BS samples after reaction and of mixtures of biochar and sulfur before reaction. The first method involved two consecutive DSC scans with the following method: (1) thermal heating from 20 °C to 200 °C at 10 °C min^{-1}; (2) isothermal holding at 200 °C for 10 minutes before heating to 220 °C at 10 °C min^{-1}; (3) isothermal holding at 220 °C for 1 minute, and (4) cooling to 20 °C at a rate of 10 °C min^{-1}. A second method was used to enhance the exothermic response of the reaction between biochar and sulfur and minimize the endothermic contributions related to sulfur polymerization. This method involved repeating three DSC cycles according to a sequence of eleven steps: (1) heating (10 °C min^{-1}) from 20 °C to 120 °C; (2) isothermal holding at 120 °C for 90 minutes; (4) heating to 200 °C at 10 °C min^{-1}; (5) cooling to 20 °C at 10 °C min^{-1}; (5) isothermal holding at 20 °C for 1 minute; (6) heating again to 200 °C at 10 °C min^{-1}; (7) isothermal holding at 200 °C for 1 minute; (8) cooling (at 10 °C min^{-1}) to 20° at 10 °C min^{-1}; (9) holding for 1 minute; followed by (10), (11) two cycles of heating and cooling from 20 °C to 200 °C at 10 °C min^{-1}, each without intermediate isothermal holds, except for a final 1-minute isothermal holding at 20 °C between cycles.

The surface morphology of the pellets was investigated by scanning electron microscopy (SEM, Quanta FEG from FEI). XRD analysis was performed using an X-ray diffractometer (Empyrean DY-2516) over a diffraction angle range of 5–80°. XRD results were obtained from room temperature to 300 °C using a nickel sample holder and a cobalt radiation source at λ = 1.79 Å and the sample was kept during heating in a controlled environment chamber. X-Ray tomography (Zeiss Xradia versa 520) was used to image the pellets at a 1.2 μm resolution and the resulting images were analyzed using the instrument's software to determine morphology, porosity, and pore size distribution. X-Ray photoelectron spectroscopy (XPS) is performed using SPECS XR50 equipped with a hemispherical energy analyzer (Phoibos 100) with Al Kα radiation at a base pressure of 1×10^{-7} Pa. All XPS spectra were analyzed and quantified with CASAXPS software. A Mercury Intrusion Porosimeter (MIP), type Micromeritics AutoPore V 9610, was used to measure the pore size distribution and porosity. The sample chamber is filled with mercury at absolute pressures of 3.58 kPa (partial vacuum) and 414 MPa, respectively. The mechanical properties were tested by axial compression, using electromechanical machine Amsler. The sample was compressed down by moving the load at a speed of 0.08 mm s^{-1} until the compressive load reached 400 kN.

5.3 Safety

The environmental impact of the biochar–sulfur reaction was evaluated by performing *in situ* analytical detection of SO_2 and H_2S emission right at the exit of the reaction chamber. For SO_2 detection, some BS(20 : 80) pellets were prepared under both nitrogen and air. The gas outlet of the reaction chamber was connected to deionized water, and the gas produced during pellet preparation was bubbled through water for the entire duration of the reaction (1 hour and 30 minutes). The pH of the collected water was measured after reaction using a pH meter. H_2S detection was made in similar conditions using a 10-ppm methylene blue solution in DI water. A UV-Vis spectrophotometer was used to detect the formation of a methylene sulfide complex in the methylene blue solution, which is at 300 nm.

Conflicts of interest

The authors declare the following competing interests: Two of the authors (C. A. and R. M.) are inventors on a provisional US Patent 63/854071 on this material composition and method.

Data availability

All data needed to evaluate the conclusions in the paper are present in the paper and SI. Additional data can be provided upon request to the corresponding author.

Supplementary information is available. See DOI: **https://doi.org/10.1039/d5mh01507c**.

Acknowledgements

The authors acknowledge the financial support of Mitacs and Elkem Biocarbone. This work was supported by the Canada Research Chair (CRC) and the Natural Sciences, Engineering Research Council of Canada (NSERC grant numbers RGPIN-2025-05339) programs. Part of this work was conducted in the shared facilities at the UdeM MIL campus, the Polytechnique Montreal (Mechanical Engineering) and the Regroupement Québécois sur les Matériaux de Pointe (RQMP). Technical support from Vincent Lemelin for XPS analysis and from François Vaillancourt for machining and fabrication is gratefully acknowledged. R. M. is a member of the RQMP and CQMF networks of the Fonds de Recherche du Québec (FRQ) (**doi.org/10.69777/309032** and **doi.org/10.69777/341666**).

References

1 IPCC special report on Carbon dioxide capture and storage,Prepared by Working Group III of the Intergovernmental Panel on Climate Change. (Cambridge University Press, 2005).
2 N. Seddon, *et al.*, Understanding the value and limits of nature-based solutions to climate change and other global challenges, *Philos. Trans. R. Soc., B*, 2020, **375**, 1–12.
3 G. V. Brigagão, J. L. de Medeiros, O. Araújo, Q. F. de, H. Mikulčić and N. Duić, A zero-emission sustainable landfill-gas-to-wire oxyfuel process: Bioenergy with carbon capture and sequestration, *Renewable Sustainable Energy Rev.*, 2021, **138**, 1–13.
4 E. Yablonovitch and H. W. Deckman, Scalable, economical, and stable sequestration of agricultural fixed carbon, *Proc. Natl. Acad. Sci. U. S. A.*, 2023, **120**, 1–6.
5 J. Lehmann, *et al.*, Biochar in climate change mitigation, *Nat. Geosci.*, 2021, **14**, 883–892.
6 W. J. Liu, H. Jiang and H. Q. Yu, Development of Biochar-Based Functional Materials: Toward a Sustainable Platform Carbon Material, *Chem. Rev.*, 2015, **115**, 12251–12285.
7 J. Wang and S. Wang, Preparation, modification and environmental application of biochar: A review, *J. Cleaner Prod.*, 2019, **227**, 1002–1022.
8 S. Kane, A. Storer, W. Xu, C. Ryan and N. P. Stadie, Biochar as a Renewable Substitute for Carbon Black in Lithium-Ion Battery Electrodes, *ACS Sustainable Chem. Eng.*, 2022, **10**, 12226–12233.
9 A. A. Shatsov, Mechanical properties of porous materials, *Met. Sci. Heat Treat.*, 2003, **45**, 441–444.
10 A. A. Firoozi, A. A. Firoozi, D. O. Oyejobi, S. Avudaiappan and E. S. Flores, Emerging trends in sustainable building materials: Technological innovations, enhanced performance, and future directions, *Results Eng.*, 2024, **24**, 1–37.
11 S. Muthukumarasamy and K. Karthik, Experimental analysis of biochar filler effects on the mechanical, water absorption, and viscoelastic properties of novel caryota fiber reinforced polymeric composites: The role of biodegradable reinforcements concentration, *Polym. Compos.*, 2025, **46**, S119–S134.
12 J. Hylton, A. Hugen, S. M. Rowland, M. Griffin and L. E. Tunstall, Relevant biochar characteristics influencing compressive strength of biochar-cement mortars, *Biochar*, 2024, **6**, 1–27.
13 M. Yang, E. Trizio and M. Parrinello, Structure and polymerization of liquid sulfur across the λ-transition, *Chem. Sci.*, 2024, **15**, 3382–3392.
14 Z. Wu and D. A. Pratt, Radical approaches to C–S bonds, *Nat. Rev. Chem.*, 2023, **7**, 573–589.
15 J. Lim, J. Pyun and K. Char, Recent approaches for the direct use of elemental sulfur in the synthesis and processing of advanced materials, *Angew. Chem., Int. Ed.*, 2015, **54**, 3249–3258.
16 M. Neurock and R. A. van Santen, Theory of Carbon-Sulfur Bond Activation by Small Metal Sulfide Particles, *J. Am. Chem. Soc.*, 1994, **116**, 4427–4439.
17 F. Qin, C. Zhang, G. Zeng, D. Huang and X. Tan, Lignocellulosic biomass carbonization for biochar production and characterization of biochar reactivity, *Renewable Sustainable Energy Rev.*, 2022, **157**, 112056.
18 S. Kloss, *et al.*, Characterization of Slow Pyrolysis Biochars: Effects of Feedstocks and Pyrolysis Temperature on Biochar Properties, *J. Environ. Qual.*, 2012, **41**, 990–1000.
19 M. Yu, T. Saunders, T. Su, F. Gucci and M. J. Reece, Effect of Heat Treatment on the Properties of Wood-Derived Biocarbon Structures, *Materials*, 2018, **11**, 1–9.
20 D. Portnikov, H. Kalman, J. S. Curtis and P. C. Pullammanappallil, Mechanical characteristics of individual bio particles, *Biomass Convers. Biorefin.*, 2020, **10**, 1207–1220.
21 A. Russell, P. Müller and J. Tomas, Quasi-static diametrical compression of characteristic elastic – plastic granules: Energetic aspects at contact, *Chem. Eng. Sci.*, 2014, **114**, 70–84.
22 B. Meyer, Elemental Sulfur, *Chem. Rev.*, 1976, **76**, 367–388.
23 M. Chase, NIST-JANAF thermochemical tables, *Am. Inst. Phys.*, 1998, 1–1951.
24 K. B. Ward and B. C. Deaton, Properties of the Group VI B Elements Under Pressure. III. Phase- Diagram Studies of Various Forms of Sulfur, *Phys. Rev.*, 1967, **153**, 947–951.
25 N. H. Meri, A. B. Aias, N. Talib, Z. A. Rashid and W. A. W. A. K. Ghani, Effect of Chemical Washing Pre-treatment of Empty Fruit Bunch (EFB) biochar on Characterization of Hydrogel Biochar composite as Bioadsorbent Effect of Chemical Washing Pre-treatment of Empty Fruit Bunch (EFB) biochar on Characterization of Hydrogel B, *Mater. Sci. Eng.*, 2018, **358**, 1–8.

26 M. Zhang, *et al.*, Size-dependent melting point depression of nanostructures: Nanocalorimetric measurements, *Phys. Rev. B: Condens. Matter Mater. Phys.*, 2000, **62**, 10548–10557.
27 Y. Namatame and H. Sato, Evaluation of polymorphic forms by powder X-ray diffraction and thermal analysis methods, *Rigaku Janaru*, 2013, **29**, 8–15.
28 A. Ray, A. Banerjee and A. Dubey, Characterization of Biochars from Various Agricultural By-Products Using Characterization of Biochars from Various Agricultural By- Products Using FTIR Spectroscopy, SEM focused with image Processing, *Int. J. Agric. Environ. Biotechnol.*, 2020, **13**, 423–430.
29 K. Jones, G. Ramakrishnan, M. Uchimiya and A. Orlov, New Applications of X-ray Tomography in Pyrolysis of Biomass: Biochar Imaging, *Energy Fuels*, 2015, **29**, 1628–1634.
30 L. Leng, *et al.*, An overview of sulfur-functional groups in biochar from pyrolysis of biomass, *J. Environ. Chem. Eng.*, 2022, **10**, 107185.
31 Q. Lian, Y. Li, K. Li, J. Cheng and J. Zhang, Insights into the Vulcanization Mechanism through a Simple and Facile Approach to the Sulfur Cleavage Behavior, *Macromolecules*, 2017, **50**, 803–810.
32 M. J. H. Worthington, R. L. Kucera and J. M. Chalker, Green chemistry and polymers made from sulfur, *Green Chem.*, 2017, **19**, 2748–2761.
33 W. J. Chung, *et al.*, The use of elemental sulfur as an alternative feedstock for polymeric materials, *Nat. Chem.*, 2013, 1–7, DOI: **10.1038/NCHEM.1624**.
34 J. J. Griebel, R. S. Glass, K. Char and J. Pyun, Polymerizations with elemental sulfur: A novel route to high sulfur content polymers for sustainability, energy and defense, *Prog. Polym. Sci.*, 2016, **58**, 90–125.
35 H. Shen, B. Zheng and H. Zhang, A Decade Development of Inverse Vulcanization Towards Green and Sustainable Practices A Decade Development of Inverse Vulcanization Towards Green and Sustainable Practices, *Polym. Rev.*, 2024, **64**, 1211–1266.
36 M. Mousavi, K. Hou, M. Kazemi, C. Li and E. H. Fini, Revolutionizing Sulfur Polymerization with a Biogenic Catalyst Approach, *Adv. Sustainable Syst.*, 2024, **2400322**, 1–11.
37 X. Wu, *et al.*, Catalytic inverse vulcanization, *Nat. Commun.*, 2019, 1–9, DOI: **10.1038/s41467-019-08430-8**.
38 Q. Hu, *et al.*, Effects of binders on the properties of biochar pellets, *Appl. Energy*, 2015, **157**, 508–516.
39 J. A. Bailey, ASM Handbook, *Mechanical Testing and Evaluation*, ASM international, Materials Par, OH, 2000, vol. 8.
40 E. G. Nawy, *Concrete Construction Engineering Handbook*, CRC Press, 2008.
41 W. D. Callister, *Materials Science and Engineering: An introduction*, John Wiley & Sons, 7th edn, 2007.
42 S. Kumar, Carbon fibre compressive strength and its dependence on structure and morphology, *J. Mater. Sci.*, 1993, **28**, 423–439.
43 P. Mehta and J. M. Monteiro, *Concrete: microstructure, properties and materials*, McGraw-Hill Education, 2006.
44 Metals Handbook, *Properties and selection: Irons, steels, and high performance alloys*, expert commitee directed by K. M. Zwilsky and E. L. Langer, ASM international, 1990.
45 Z. Miao, P. Zhang, M. Li, Y. Wan and X. Meng, Briquette preparation with biomass binder, *Energy Sources, Part A*, 2023, **45**, 9834–9844.

